GRAPHENE

Detection of graphene's divergent orbital diamagnetism at the Dirac point

J. Vallejo Bustamante[1], N. J. Wu[1,6], C. Fermon[2], M. Pannetier-Lecoeur[2], T. Wakamura[1,7], K. Watanabe[3], T. Taniguchi[4], T. Pellegrin[1], A. Bernard[1], S. Daddinounou[1], V. Bouchiat[5], S. Guéron[1], M. Ferrier[1], G. Montambaux[1], H. Bouchiat[1]*

The electronic properties of graphene have been intensively investigated over the past decade. However, the singular orbital magnetism of undoped graphene, a fundamental signature of the characteristic Berry phase of graphene's electronic wave functions, has been challenging to measure in a single flake. Using a highly sensitive giant magnetoresistance (GMR) sensor, we have measured the gate voltage–dependent magnetization of a single graphene monolayer encapsulated between boron nitride crystals. The signal exhibits a diamagnetic peak at the Dirac point whose magnetic field and temperature dependences agree with long-standing theoretical predictions. Our measurements offer a means to monitor Berry phase singularities and explore correlated states generated by the combined effects of Coulomb interactions, strain, or moiré potentials.

Orbital magnetism results from the quantum motion of electrons in a magnetic field. At low energy, this motion leads to the Landau spectrum, which is, in most two-dimensional (2D) conductors, a harmonic oscillator–type spectrum with equally spaced levels separated by the cyclotron energy $\hbar\omega_c$ (*1*). As long as the material is nonsuperconducting, this spectrum causes a very small diamagnetic low-field susceptibility that is usually hidden by spin contributions. However, some materials, such as graphene, can display extraordinarily large diamagnetism. This was predicted in the theoretical work of McClure (*2*), who showed that graphene is diamagnetic at half filling (at the so-called Dirac point), with a divergent zero-field susceptibility (the derivative of the magnetization M with respect to the magnetic field B),

$$\chi_0(\mu) = \frac{\partial M}{\partial B} = -\frac{2e^2 v_F^2}{3\pi}\delta(\mu) \qquad (1)$$

where v_F is the Fermi velocity, e is the electronic charge, and the Fermi energy μ is zero at the Dirac point. This is all the more surprising because the density of states is zero at that point. The reason for this singular susceptibility stems from the electron-hole symmetric linear spectrum of Dirac relativistic electrons, which gives rise to a Landau spectrum quantized as $\pm\sqrt{nB}$ where n is a positive integer. The diamagnetic sign of the response is attributable to the existence of the zero-energy Landau level ($n = 0$), as recalled and sketched below [see also figure 5 of (*3*) and related comment]. This peculiar level is known to result from the Berry phase (*4*) of π acquired by the wave function pseudo-spin upon a revolution around a Dirac cone in reciprocal space (*5*). Therefore, the diamagnetic sign of the susceptibility at the Dirac point is a direct consequence of the π Berry phase. Indeed, it has been shown that slightly different models with a zero Berry phase lead to orbital paramagnetism at the Dirac point (*3*). To summarize, the divergence reflects the linear spectrum and the diamagnetic sign reflects the nontrivial geometry of the eigenstates via the Berry phase (*3*).

However, despite these striking predictions, the singular orbital magnetism of a single graphene flake remains undetected. The reason for this lies in at least three obvious experimental challenges. First, the magnetic signal of an atomic monolayer is extremely small. Second, the McClure singularity, originally computed for an ideal system without disorder at zero temperature and in the limit of zero magnetic field, is rounded when any of these conditions is relaxed (*6*–*9*). Finally, this orbital magnetism is expected to be hidden by the magnetism of spins originating from edges, vacancies, or impurities (*10*), which tends to become dominant at low temperatures. This may explain why magnetization measurements have to date only been performed on a macroscopic number of graphene flakes. In one case (*11*), the focus was mainly on the spin paramagnetism of induced vacancy– and resonant states–type defects, which were found to depend on the chemical doping of the samples. A second set of measurements (*12*) did focus on the diamagnetism, and found a diamagnetism larger than that of pure graphite by a factor of 3. The magnetization curves at high fields were found to be compatible with the $\sqrt{B}$ dependence predicted for the Dirac spectrum. However, in those experiments it was not possible to fix the doping, nor could the residual contribution of paramagnetic spins along the edges of the flakes be well controlled (*13*).

In the present experiment, by contrast, we measure the orbital moment of a single flake whose Fermi energy is precisely controlled. This is achieved by implementing several sensitivity-enhancing features detailed in (*14*). As shown in Fig. 1, our experiment consists of a graphene monolayer, encapsulated between two hexagonal boron nitride (hBN) 2D crystals, capacitively coupled to a top-gate electrode and positioned above a highly sensitive magnetic detector made of two giant magnetoresistance (GMR) strips (figs. S1 to S3) in a Wheatstone bridge configuration. One key asset is that whereas graphene's orbital magnetism responds to a field perpendicular to the graphene plane ("vertical" field), the resistance of the GMR detectors only depends on the in-plane field, and thus detects the horizontal component of the field generated by the orbital current loops in the graphene (Fig. 1), all the while being insensitive to the applied vertical field. A second feature is the addition of a small AC modulation to the DC gate voltage, which in turn modulates the magnetization with respect to gate voltage and thus the resistance of the GMR detector. Beyond increasing the sensitivity, this modulation technique makes gate-independent magnetic signals invisible. Thanks to these experimental implementations, we were able to detect the derivative with respect to gate voltage of the diamagnetic McClure peak at low magnetic fields. We have also measured the crossover to the de Haas–van Alphen magnetic oscillations at higher fields.

Figure 2 shows the gate voltage derivative of the field induced by the graphene sample on the calibrated GMRs as a function of V_g for perpendicular magnetic fields between 0.1 and 1.2 T. We found an antisymmetric peak centered at $V_g = -0.29$ V, which we identified as the Dirac point by comparing to the position of the maximum in the resistance of the sample $R(V_g)$ (Fig. 2B and fig. S3). At low magnetic fields, the antisymmetric peak detected in the GMR resistance is directly proportional to the derivative of the McClure peak with respect to the chemical potential (controlled by the gate voltage), as detailed in (*14*). The experimental detection of this peak and its evolution with magnetic field are the central result of our work. Both the peak width and amplitude increase linearly with field, as shown in Fig. 2, E and F. Above 0.6 T, $\partial M/\partial V_g(V_g)$ displays periodic oscillations in addition to the antisymmetric

[1]Université Paris-Saclay, CNRS, Laboratoire de Physique des Solides, 91405 Orsay, France. [2]SPEC, CEA, CNRS, Université Paris-Saclay, 91191 Gif-sur-Yvette, France. [3]Research Center for Functional Materials, National Institute for Materials Science, 1-1 Namiki, Tsukuba 305-0044, Japan. [4]International Center for Materials Nanoarchitectonics, National Institute for Materials Science, 1-1 Namiki, Tsukuba 305-0044, Japan. [5]Néel Institute, CNRS, 38000 Grenoble, France. [6]Université Paris-Saclay, CNRS, Institut des Sciences Moléculaires d'Orsay, Orsay, France. [7]NTT Basic Research Laboratories, NTT Corporation, Atsugi, Kanagawa, Japan.
*Corresponding author. Email: helene.bouchiat@u-psud.fr

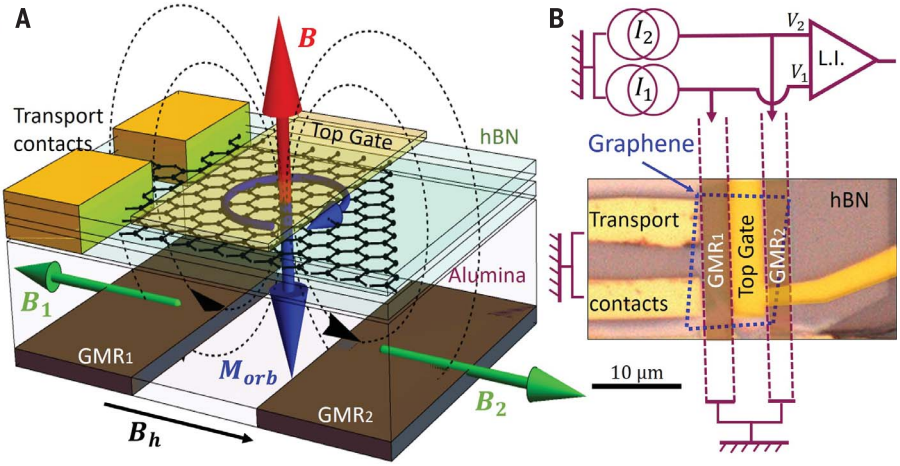

Fig. 1. Experimental setup. (**A**) Principle of the experiment. The orbital magnetization M_{orb} can be viewed as a current loop (blue circle) generated by a vertical magnetic field B and circulating around the graphene region covered by the gate electrode. It is detected by the two GMR detectors, which measure the horizontal components B_1 and B_2 (respectively on the detectors GMR_1 and GMR_2) of the magnetic field (black dashed lines) generated by this loop. The sensitivity is on the order of 0.1 nT (*14*). (**B**) Micrograph of the sample investigated; the gate voltage derivative of the orbital magnetization is measured via the difference between the DC current–biased GMR_1 and GMR_2 resistances with I_1 and I_2 adjusted so as to cancel the DC component of the voltage difference $V_1 - V_2$. The signal measured by a lock-in amplifier (L.I.) is the AC component of $V_1 - V_2$ at the modulation frequency of the gate voltage. There is no current applied to the graphene sample during the magnetization measurements.

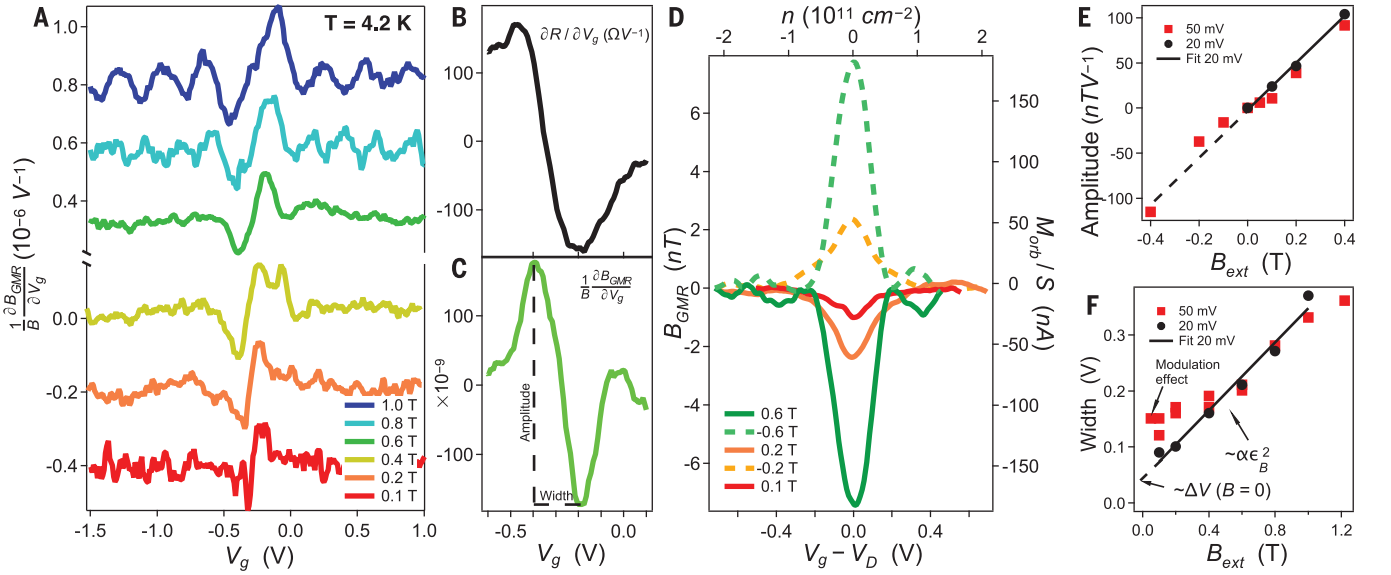

Fig. 2. Magnetization data. (**A**) Detected modulation of the GMR detector's resistance with an AC gate voltage modulation of 20 mV, as a function of the DC gate voltage V_g. The quantity plotted is $\partial B_{GMR}/\partial V_g$, where B_{GMR} is deduced from the signal on the calibrated GMR sensor divided by the applied vertical magnetic field B. Data are the average of 80 independent measurements. (**B**) Derivative with respect to gate voltage of the two-point resistance of graphene measured through the side electrodes, in the region of the Dirac point, with a gate voltage modulation of 50 mV. (**C**) For comparison, the GMR signal at −0.6 T using the same gate voltage modulation as in (B). The GMR peak is much narrower. (**D**) Numerical integration of the data plotted in (A) and fig. S4, yielding the magnetization per unit surface (in nA; right axis) and the magnetic field B_{GMR} detected by the GMR device (in nT; left axis) as a function of the gate voltage. (**E** and **F**) Field dependences of the GMR peak maxima and widths, as defined in (C), for gate voltage modulations of 20 mV (circles) and 50 mV (squares), and comparison with the linear variations expected theoretically (see Eqs. 5 and 6 and eqs. S20 to S27), using the scaling between the gate voltage and the square of the Landau energy ε_B^2 via the parameter α defined in Eq. 8. Deviations from linearity caused by excessive modulation amplitudes are visible for a 50-mV modulation.

peak around the Dirac point. These oscillations are related to the expected de Haas–van Alphen oscillations of the magnetization, as discussed below.

The magnetization, shown in Fig. 2D, is obtained by the integration of the curves in Fig. 2A. The peak amplitude translates into a few nanoteslas induced in the GMR plane by graphene's orbital response to a 0.1-T perpendicular field. This illustrates the sensitivity of our experiment. The correspondence between this detected field, B_{GMR}, and magnetization is obtained by modeling the orbital magnetic moment as an effective current loop whose geometry is defined by the gated region of graphene (fig. S10). We find that positive magnetic fields produce a negative peak in magnetization, and vice versa, which is consistent with the expected diamagnetic response of graphene (*2*). The sign of the response was carefully determined via the sign of the response of the GMR sensor to a horizontal field of known orientation. We can assert that the signal cannot be attributed to gate voltage–dependent magnetism of paramagnetic impurities, given the absence of temperature dependence between 4.2 and 40 K (*15*) (see fig.

S9). In addition, thanks to our gate modulation technique, we can exclude spurious contributions from impurities or defects in alumina or graphene, which would not depend on gate voltage. This contrasts with all previous measurements of graphene's magnetism, which were performed on large ensembles of flakes.

In the following, we compare our results to theoretical predictions, taking into account the variations of the chemical potential caused by charge inhomogeneity, and ignoring the smaller broadening due to temperature (*14*). Assuming a Gaussian distribution for the electrochemical potential μ′ of standard deviation σ,

$$P_\sigma(\mu') = \frac{1}{\sqrt{2\pi}\sigma}\exp\left(-\frac{\mu'^2}{2\sigma^2}\right) \quad (2)$$

yields a smoothed susceptibility,

$$\chi_\sigma(\mu) = \int P_\sigma(\mu')\chi_0(\mu-\mu')d\mu' \quad (3)$$

Then, the δ-peak of the susceptibility is broadened as

$$\chi_\sigma(\mu) = -\frac{2e^2v_F^2}{3\pi}P_\sigma(\mu) \quad (4)$$

The full field and chemical potential dependence of the magnetization, including the oscillations, is given by the derivative $M = -\partial\Omega/\partial B$ of the disorder-averaged grand potential $\Omega_\sigma(\mu, B)$ (*14*) (eqs. S20 to S23):

$$\Omega_\sigma(\mu,B) = \int P_\sigma(\mu')\Omega_0(\mu-\mu',B)d\mu' \quad (5)$$

with

$$\Omega_0(\mu,B) = \frac{\varepsilon_B^3}{4\pi^2\hbar^2c^2}\sum_{p>0}\frac{1}{p^{3/2}}\left[1-2S\left(2\sqrt{p}\frac{|\mu|}{\varepsilon_B}\right)\right] \quad (6)$$

The Landau levels at energies $\sqrt{n}\varepsilon_B$, with $\varepsilon_B = \sqrt{2e\hbar v_F^2 B}$, enter via the argument $\sqrt{p}|\mu|/\varepsilon_B$ where p is an integer, in the Fresnel function

$$S(x) = \int_0^x \sin\frac{\pi}{2}t^2dt \quad (7)$$

The predicted disorder-averaged magnetization is displayed in Fig. 3E. With increasing field, it evolves from a sole diamagnetic McClure peak of width σ to a broader peak with additional oscillations, centered at $\mu_n/\varepsilon_B = \sqrt{n}$. Figure 3D demonstrates how charge disorder induces rounding and attenuates the oscillations.

To compare these predictions to experiment, we must also relate the gate voltage V_g to the chemical potential μ. Far from the Dirac point, this relation is quadratic, $V_g(\mu) - V_D = \alpha\mu^2\,\mathrm{sign}(\mu)$, with

$$\alpha = \frac{e/C_g}{\pi\hbar^2v_F^2} \quad (8)$$

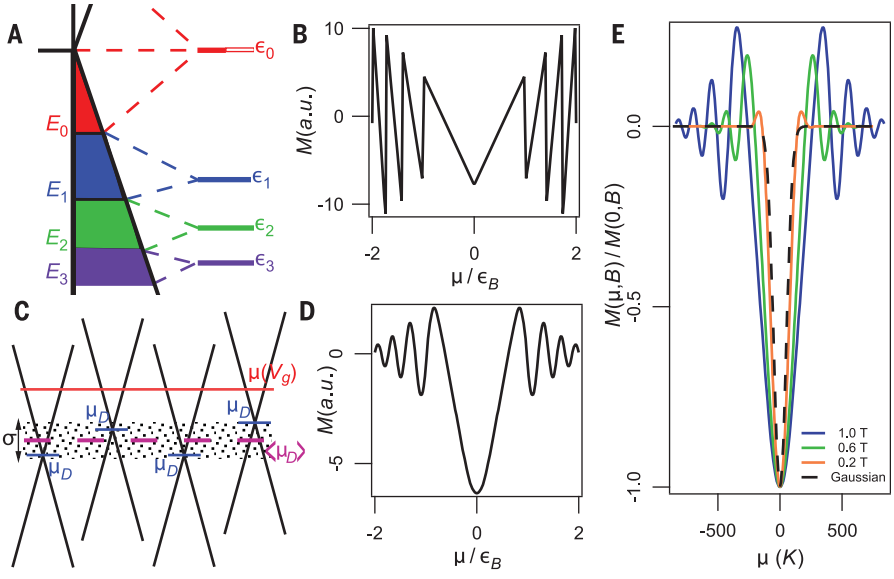

Fig. 3. Calculated chemical potential dependence of the orbital magnetization of graphene in a finite magnetic field. The calculations are based on Eq. 6; see (*14*) for more details. (**A**) Evolution of the graphene spectrum in a magnetic field [adapted from (*3*)]. The condensation of the continuous spectrum into Landau levels decreases the energy, except for the zero energy level whose contribution is predominant. Globally, the net result is an increase of the energy with the field—that is, a diamagnetic response [see also figure 5 of (*3*)]. (**B**) Without disorder, the magnetization, plotted as a function of the rescaled chemical potential μ/ε_B, exhibits discontinuities at the Landau level energies $\sqrt{n}\varepsilon_B$; a.u., arbitrary units. (**C**) Sketch illustrating the spatial distribution of electrochemical potentials $\mu' = \mu_D - \langle\mu_D\rangle$ where μ_D is the local Dirac point and $\langle\mu_D\rangle$ is its spatial average. (**D**) Rounding of $M(\mu/\varepsilon_B)$ by a Gaussian chemical potential distribution with a variance $\sigma = 0.1\varepsilon_B$. (**E**) Calculated $M(\mu)$ for different magnetic fields for σ = 50 K. At low fields, the oscillations disappear and the magnetization displays a Gaussian diamagnetic peak at μ = 0. This peak is broadened by the magnetic field as soon as $\varepsilon_B \geq \sigma$.

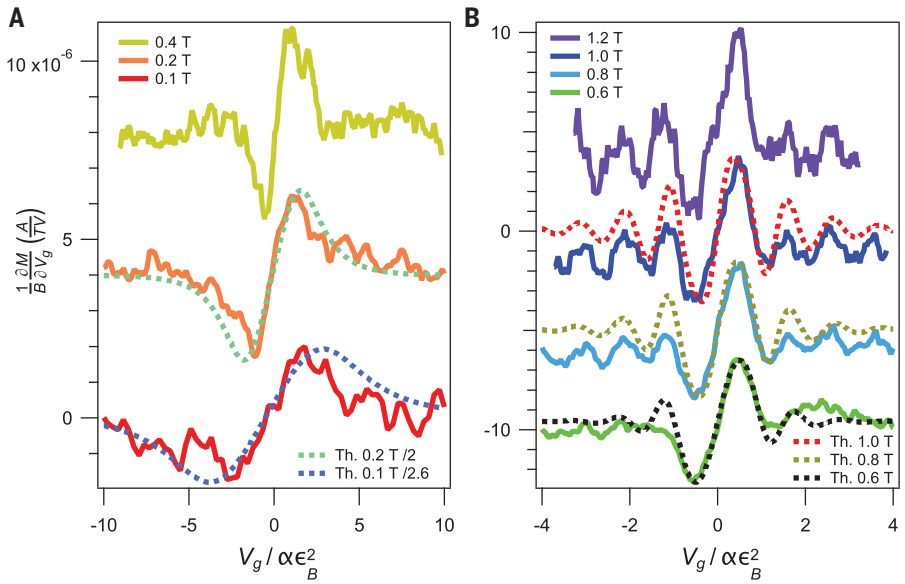

Fig. 4. Comparison of theory to experiment. Fit of detected AC magnetization response to a gate voltage modulation of 50 mV, as a function of the DC gate voltage divided by $\alpha\varepsilon_B^2 = 2\alpha e\hbar v_F^2 B$. Dashed lines show the theoretical gate dependence of $\partial M/\partial V_g$, with σ_0 = 165 K and σ_∞ = 50 K, including the extra rounding effect owing to the 50-mV AC gate modulation. In (**A**), the amplitude of the theoretical signal has been rescaled by a factor of 1/2.6 at 0.1 T and by a factor of 1/2 at 0.2 T to fit quantitatively the experimental data. In (**B**), the rescaling factors are closer to unity for higher fields for which the McClure peak is expected to be independent of σ_0.

where V_D is the gate voltage at the Dirac point, and C_g is the geometrical capacitance per unit surface between graphene and gate, as determined from the V_g periodicity of the de Haas–van Alphen oscillations at high field (*14*). In contrast, close to the Dirac point, V_g varies linearly with μ, with a slope given by the standard deviation of μ disorder around the Dirac point, σ_0:

$$V_g(\mu) - V_D = \frac{4\sigma_0\mu}{\sqrt{2\pi}} \qquad (9)$$

(eqs. S24 and S25). We find that the experimental data can be fit (see Fig. 4) using two constants, σ_0 = 165 K and σ_∞ = 50 K, which describe the μ distribution at low and high doping respectively (eqs. S26 and S27). The smaller value of σ_∞ is explained by the more efficient screening of charge impurities at high doping. We note that the two constants can practically be determined independently, given the high sensitivity of the decay of the de Haas–van Alphen oscillations to disorder, and the large broadening of the McClure peak induced by magnetic field (on the order of ε_B).

We find that $M(V_g)$ and $\partial M/\partial V_g$ depend on V_g, σ_0, and σ_∞, exclusively via the variables $V_g/\alpha\varepsilon_B^2$, σ_0/ε_B, and $\sigma_\infty/\varepsilon_B$. In particular, the variation as $\alpha\varepsilon_B^2$ of the $\partial M/\partial V_g$ peak's width, shown in Fig. 2F, is directly related to this scaling, which originates from the Dirac Landau spectrum of graphene.

Next, we compare the magnetization peaks measured at the Dirac point at 0.1 T and 0.2 T to theoretical expectations. We find that the predicted amplitude of the antisymmetric magnetization peak at the Dirac point $(1/B)(\partial M/\partial V_g)$ at low magnetic field, equal to $9.6 \times 10^{-6}\, A(TV)^{-1}$, is on the order of the experimental values, although larger by a factor 2 to 2.6. This is probably a consequence of the oversimplified model of the Gaussian distribution of electrochemical potentials we have used. This value corresponds to a diamagnetic magnetization two orders of magnitude larger than the Landau diamagnetism of a 2D free electron gas. Finally, deviations from the linearity between magnetization and magnetic field are expected when ε_B becomes much greater than σ_0, with a smooth crossover toward a $\sqrt{B}$ dependence (eqs. S20 to S23). Because the calibration of the GMR sensor becomes delicate in high perpendicular magnetic fields owing to the residual imperfect alignment of the magnetic field, these deviations from linearity cannot be precisely checked in the field range above 0.5 T where they are expected to occur.

We have detected the McClure singularity of low-field orbital magnetization of a single graphene monolayer at the Dirac point, which is the signature of the π Berry phase of electronic wave functions in graphene. This experiment should also enable the investigation of interband-induced Berry curvature anomalies (*16*–*18*) as well as Coulomb interaction effects in 2D materials such as graphene and its bilayer (*19*, *20*). Moreover, in contrast to the diamagnetic McClure peak observed here, a divergent paramagnetic orbital susceptibility (*21*) is expected at Van Hove singularities in the presence of moiré potentials of high periodicity. These moiré potentials also generate flat bands in the magic-angle twisted bilayer of graphene (*22*). An anomalous quantum Hall effect is then expected to appear as the result of Coulomb interactions leading to valley symmetry breaking (*23*–*25*) and orbital current loops in zero magnetic field. They are detectable via the orbital magnetic moments they would generate, as very recently shown in (*26*). The possibility of generating flat bands with a periodic array of strain has also been predicted (*27*–*29*). In fig. S12, we present data on a strained sample on which it was possible to detect a gate-dependent GMR signal at zero magnetic field. This preliminary result suggests that more controlled situations like that in (*30*) can be investigated. Such measurements could also be used to reveal the expected ballistic loop currents along the edges of 2D topological insulators (*31*–*34*).

REFERENCES AND NOTES

1. L. D. Landau, *Eur. Phys. J. A* **64**, 629–637 (1930).
2. J. W. McClure, *Phys. Rev.* **104**, 666–671 (1956).
3. A. Raoux, M. Morigi, J.-N. Fuchs, F. Piéchon, G. Montambaux, *Phys. Rev. Lett.* **112**, 026402 (2014).
4. M. V. Berry, *Proc. R. Soc. London Ser. A* **392**, 45–57 (1984).
5. H. Castro Neto, F. Guinea, N. M. R. Peres, K. S. Novoselov, A. K. Geim, *Rev. Mod. Phys.* **81**, 109 (2009).
6. H. Fukuyama, *Prog. Theor. Phys.* **45**, 704–729 (1971).
7. H. Fukuyama, *J. Phys. Soc. Jpn.* **76**, 043711 (2007).
8. M. Koshino, T. Ando, *Phys. Rev. B* **76**, 085425 (2007).
9. Y. Ominato, M. Koshino, *Phys. Rev. B* **87**, 115433 (2013).
10. O. V. Yazyev, *Rep. Prog. Phys.* **73**, 056501 (2010).
11. R. R. Nair *et al.*, *Phys. Rev. Lett.* **105**, 207205 (2010).
12. Z. Li *et al.*, *Phys. Rev. B* **91**, 094429 (2015).
13. L. Chen *et al.*, *RSC Adv.* **3**, 13926 (2013).
14. See supplementary materials.
15. J. H. Chen, L. Li, W. G. Cullen, E. D. Williams, M. S. Fuhrer, *Nat. Phys.* **7**, 535–538 (2011).
16. D. Xiao, M. C. Chang, Q. Niu, *Rev. Mod. Phys.* **82**, 1959–2007 (2010).
17. A. Raoux, F. Piéchon, J.-N. Fuchs, G. Montambaux, *Phys. Rev. B* **91**, 085120 (2015).
18. A. Raoux, thesis, Université Paris Saclay (2017).
19. L. Ju *et al.*, *Science* **358**, 907–910 (2017).
20. A. Principi, M. Polini, G. Vignale, M. I. Katsnelson, *Phys. Rev. Lett.* **104**, 225503 (2010).
21. G. Vignale, *Phys. Rev. Lett.* **67**, 358–361 (1991).
22. Y. Cao *et al.*, *Nature* **556**, 80–84 (2018).
23. A. L. Sharpe *et al.*, *Science* **365**, 605–608 (2019).
24. M. Serlin *et al.*, *Science* **367**, 900–903 (2020).
25. J. Liu, Z. Ma, J. Gao, X. Dai, *Phys. Rev. X* **9**, 031021 (2019).
26. C. L. Tschirhart *et al.*, *Science* **372**, 1323–1327 (2021).
27. J. W. F. Venderbos, L. Fu, *Phys. Rev. B* **93**, 195126 (2015).
28. C. C. Hsu, M. L. Teague, J. Q. Wang, N. C. Yeh, *Sci. Adv.* **6**, eaat9488 (2020).
29. Y. Zhang *et al.*, *Phys. Rev. B* **102**, 081403 (2020).
30. A. Reserbat-Plantey *et al.*, *Nano Lett.* **14**, 5044–5051 (2014).
31. C. L. Kane, E. J. Mele, *Phys. Rev. Lett.* **95**, 226801 (2005).
32. T. Yoda, T. Yokoyama, S. Murakami, *Sci. Rep.* **5**, 12024 (2015).
33. P. Potasz, J. Fernández-Rossier, *Nano Lett.* **15**, 5799–5803 (2015).
34. H. Kim *et al.*, *NPG Asia Mater.* **8**, e271 (2016).
35. J. Vallejo, Zenodo (2021); https://zenodo.org/record/5541353#.YW0rIF5R1PY.

ACKNOWLEDGMENTS

We thank E. Paul of SPEC-CEA for the GMR sensors patterning, and R. Deblock, A. Chepelianskii, F. Piéchon, J. N. Fuchs, F. Parmentier, R. Delagrange, A. Murani, and S. Sengupta for fruitful discussions. **Funding:** Supported by the BALLISTOP ERC 66566 advanced grant and the MAGMA ANR-16-CE29-0027-01 grant. Also supported by the Elemental Strategy Initiative conducted by the MEXT, Japan, grant JPMXP0112101001, JSPS KAKENHI grant JP20H00354, and CREST (JPMJCR15F3), JST (K.W. and T.T.). **Author contributions:** J.V.B. fabricated and positioned the graphene stack on the GMR device, optimized and ran the experiment, and worked on the interpretation and fits of the data. N.J.W. and T.W. helped on sample fabrication. K.W. and T.T. provided hBN single crystals. T.P., A.B., S.D., and V.B. contributed to the design, optimization, and calibration of the experiment. C.F. and M.P.-L. designed, fabricated, and optimized the GMR sensors. G.M. is responsible for the theoretical part of the work. M.F., S.G., and H.B. supervised the experimental work. J.V.B., T.W., C.F., M.P.-L., G.M., S.G., and H.B. contributed to the writing of the manuscript. **Competing interests:** There are no competing interests. **Data and materials availability:** Datasets and theory curves computed using mathematica are available on Zenodo (*35*).

SUPPLEMENTARY MATERIALS

science.org/doi/10.1126/science.abf9396
Materials and Methods
Supplementary Text
Figs. S1 to S17
References (*36*–*44*)

10 December 2020; resubmitted 14 August 2021
Accepted 19 October 2021
10.1126/science.abf9396

Detection of graphene's divergent orbital diamagnetism at the Dirac point

J. Vallejo Bustamante, N. J. Wu, C. Fermon, M. Pannetier-Lecoeur, T. Wakamura, K. Watanabe, T. Taniguchi, T. Pellegrin, A. Bernard, S. Daddinounou, V. Bouchiat, S. Guéron, M. Ferrier, G. Montambaux, and H. Bouchiat

Science **374** (6573), . DOI: 10.1126/science.abf9396

Detecting orbital magnetism

Graphene's electronic structure has been predicted to lead to an unusual orbital response to magnetic fields. However, detecting this orbital magnetism is difficult because it is usually masked by the signal stemming from spins. Vallejo Bustamante *et al*. managed to capture this response by placing two giant magnetoresistance detectors below a sample of graphene sandwiched by layers of hexagonal boron nitride. These detectors picked up a strong diamagnetic response from an undoped sample, consistent with theoretical predictions. The technique may be useful in the investigation of other two-dimensional materials. —JS